Energies **2015**, *8*, 2587-2605; doi:10.3390/en8042587

OPEN ACCESS

energies

ISSN 1996-1073

www.mdpi.com/journal/energies

Article

Effects of Electric Fields on the Combustion Characteristics of Lean Burn Methane-Air Mixtures

Jianfeng Fang [1], Xiaomin Wu [1,2,*], Hao Duan [1], Chao Li [1] and Zhongquan Gao [1]

[1] Institute of Internal Combustion Engine, Xi'an Jiaotong University, Xi'an 710049, China; E-Mails: fangjianfeng981120@163.com (J.F.); walry7518@stu.xjtu.edu.xn (H.D.); wzer1987@stu.xjtu.edu.cn (C.L.); gaozq@mail.xjtu.edu.cn (Z.G.)

[2] Key Laboratory of Shaanxi Province for Industrial Automation, Shaanxi University of Technology, Hanzhong 723001, China

* Author to whom correspondence should be addressed; E-Mail: xmwu@mail.xjtu.edu.cn; Tel.: +86-29-8266-8721; Fax: +86-29-8266-8789.

Academic Editor: Thomas E. Amidon

Received: 18 January 2015 / Accepted: 24 March 2015 / Published: 31 March 2015

Abstract: In this work, the effects of the electric fields on the flame propagation and combustion characteristics of lean premixed methane–air mixtures were experimentally investigated in a constant volume chamber. Results show that the flame front is remarkably stretched by the applied electric field, the stretched flame propagation velocity and the average flame propagation velocity are all accelerated significantly as the input voltage increases. This indicates that the applied electric field can augment the stretch in flame, and the result is more obvious for leaner mixture. According to the analyses of the combustion pressure variation and the heat release rate, the peak combustion pressure P_{max} increases and its appearance time t_p is advanced with the increase of the input voltage. For the mixture of $\lambda = 1.6$ at the input voltage of −12 kV, P_{max} increases by almost 12.3%, and t_p is advanced by almost 31.4%, compared to the case of without electric fields. In addition, the normalized mass burning rate and the accumulated mass fraction burned are all enhanced substantially, and the flame development duration and the rapid burning duration are remarkably reduced with the increase of the input voltage, and again, the influence of electric field is more profound for leaner mixtures. The results can be explained by the electric field-induced stretch effects on lean burn methane-air mixture.

Keywords: electric field; flame propagation speed; electrically induced stretch; lean burn mixture; combustion pressure; heat release rate

1. Introduction

It is well known that radical ions, such as CH_3^+, H_3O^+, $C_3H_3^+$, CHO^+ and electrons are produced during combustion using hydrocarbons as fuel, so the application of an electric field can strongly influence the flame front behavior and the combustion characteristics. Significant efforts have been made to study the effects of externally applied electric fields on the combustion process. In those studies, various types of flames have been studied, such as Bunsen flame [1–4], jet flame [5,6], flat flame [7], tribrachial flow flame [8], *etc.* Meanwhile, both direct current (DC) [9–16] and alternating-current (AC) [17–21] electric fields have been utilized. Through electrically enhanced combustion, stabilized flames [2,13], reduced carbon formation [18] and increased flame velocity [10,14,15] are among the main effects that have been observed.

Regarding electrically enhanced combustion, so-called ionic wind effects, *i.e.*, a result of a body force acting on charged particles through electric field, is a well-known phenomenon. The electric field force generates the mass transfer of ions in the field direction and produces an acceleration of neutral molecules with which the ions collide. The ionic wind effect is mainly used to illuminate the interaction between a weak electric field and flame propagation behavior at low electric power consumption. Another different way of applying electricity to flames involves the operation of corona discharges. In this case, the electrical discharging atmosphere contains high-energy electrons, such as plasmas, and can have great effect on combustion characteristics. However, the operation in a corona mode will require up 500 times more electric power than exploiting the ionic wind mechanism [22].

As far as we are concerned, the studies of the effects of electric fields on combustion are primarily concentrated on stationary flames, while little work was reported on the effects of the electric field on the outwardly propagating spherical flame. In fact, the combustion statuses of a homogeneous mixture in a constant volume bomb show similar behavior to the combustion process in the internal combustion (IC) engines, and investigating its burning characteristics is an effective means for enhancing IC engine thermal efficiency and reducing emissions. Moreover, the spherical flame can be easily determined the flame laminar burning velocity owing to its simple combustion geometry. The laminar velocities are fundamentally important in regard to developing and justifying the chemical kinetic mechanisms, as well as in regard to predicting the performance of combustion systems. In recent years, Shinichi [14] studied the relationship between a corona discharge and flame propagation behavior by using a constant volume vessel and found that the premixed flame propagated faster with the increase of the input voltage. Cha [23] investigated the premixed combustion under an AC electric field based on the spherical flame pattern and reported that the flame surface was more wrinkled and the flame propagation speed was enhanced under the applied electric field, while the overall burning rates were not much affected. Meng [24] studied the effects of DC electric fields on the combustion characteristics of the spherically expanding flames and reported that the electric fields could increase the flame propagation and shorten the overall combustion duration. In addition, the combustion pressure and the

rate of pressure rise were increased during the early stage of combustion. However, previous works concentrated on propane-air flames and methane-air flames, and mainly supplied information at near stoichiometric equivalence ratios. There are still many aspects that require investigation, especially over wide ranges of lean burning conditions. Researching combustion characteristics in fuel lean mixtures is very important to enhance the IC engine combustion and reduce toxic pollutant formation. Additionally, the understanding of the analysis on the modification of flame responses and structure under the electric field would be a benefit. Especially research on the response time [25,26] of the flame can give information about how fast the electric field can be applied to control a flame, which is important for technical applications. The objective of this paper is to study the effects of the electric fields on premixed methane–air combustion under lean conditions based on the spherical flame pattern. In the following, the experiments will be briefly specified, followed by the experimental observations of the flame propagation under the elevated electric field intensity. Additionally, the pressure evolution and the heat release rate will also be presented to further demonstrate the electric field effects. The analysis will provide more information about the effects of the electric fields on combustion characteristics.

2. Experimental Methods

2.1. Experimental Setup and Procedures

The experimental system is sketched in Figure 1. It consists of a constant volume combustion chamber, the ignition control, fuel supply, electric field generation, data acquisition and a high-speed schlieren photography system. The combustion chamber is a cylinder type with an inner diameter of 130 mm and a length of 130 mm. An insulating bush made of the polytetrafluoroethylene (PTFE) with an inner diameter of 115 mm, a thickness of 7.5 mm and a length of 130 mm is installed inside the combustion chamber. Two quartz windows with a 145 mm diameter are mounted on two sides of the bomb to allow optical accessibility. The ignition electrodes are located in the vertical direction along the bomb centerline and are surrounded by the PTFE to insulate the electrics. The high-voltage electrodes applying an electric field inside the combustion chamber, are a pair of stainless steel straight needles with a diameter of 4 mm, and are opposing located in the horizontal direction along the bomb centerline, 35 mm away from the bomb center, respectively. The outside surface of the needle is very smooth, and there are not sharp edges at the needle tip to avoid discharge at high input voltage. The power supply (DEL30N45, Weisiman company, Xianyang, China) connected to the high-voltage electrode has the output range between 0 and 30 kV. In the experiment, a high-speed digital camera (HG-100K) operating at 10,000 frames per second is used to take photos of the flames during the flame propagation. The piezo-electric Kistler absolute pressure transducer (Kistler Instruments Gmbh, Ostfildern, Germany) with an accuracy of 0.01 kPa is applied to record the combustion pressure. Methane and air are supplied into the chamber sequentially and their partial pressures are determined by the desired excess air ratio λ and the total initial pressure. Five minutes are waited before starting the ignition to ensure the homogeneity of the methane–air mixtures. The excess air ratio is defined as $\lambda = m_{air}/m_{stoic}$, where m_{air}, and m_{stoic} are the air masses needed in burn 1 kg fuel actually and theoretically, respectively. For fuel-rich mixtures, $\lambda < 1$, and for fuel-lean mixture, $\lambda > 1$. In the case of a stoichiometric mixture, λ equals unity.

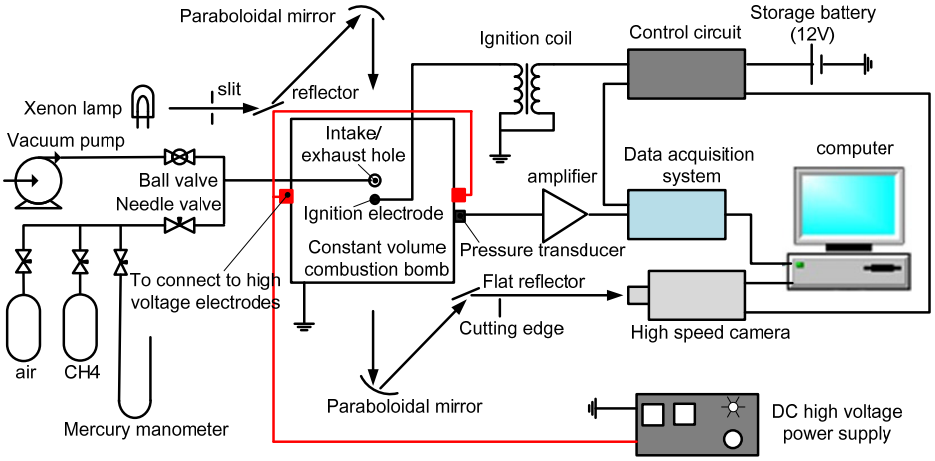

Figure 1. Schematic of experimental system.

Figure 2 shows the schematic diagram of the constant volume combustion chamber arrangements with the high-voltage electrodes and the ignition electrodes. In the experiment, four electric voltages (0, −5, −10, −12 kV) are applied to produce the electric fields across the flames. The methane–air mixture is prepared at three excess air radios of 1.2, 1.4 and 1.6, and it is charged in the combustion chamber at room temperature and atmospheric pressure. For the experimental system, the input voltage for breakdown of the flame gas between the high-voltage electrode and the ignition electrode is about −18 kV. While the maximum voltage applied in the experiments is −12 kV, and the electric power does not exceed 0.1% of the thermal power. Thus, the gas discharges are not likely to occur under these conditions. Each experiment is repeated at least three times under the same conditions and excellent repeatability is achieved.

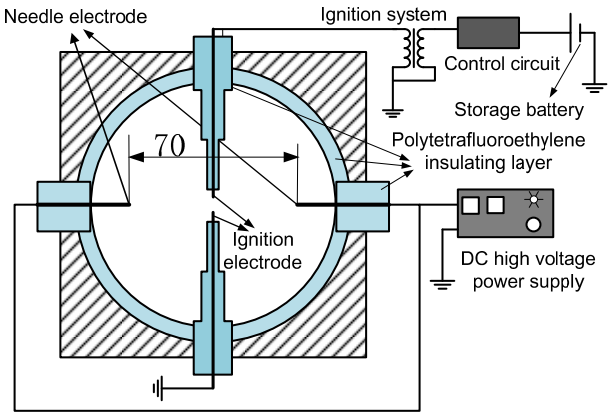

Figure 2. Structure of the constant volume combustion chamber.

2.2. Calculation of Heat Release Rate

To extract information on the combustion process, a cycle-resolve mass burning rate calculation is performed using a quasi-dimensional two-zone combustion model. Assuming the flame front is a thin, reactive sheet, the model divides the combustion chamber into two zones, *i.e.*, burned zone and unburned zone, and is based on the following assumptions:

1 The mixture will be burned immediately after entering the flame region.
2 The burned gas within the flame kernel is in chemical equilibrium.
3 The pressure is uniform throughout the burned and unburned zone.

Then, the mass and energy conservation yield:

$$\frac{\mathrm{d}m_\mathrm{u}}{\mathrm{d}t} = -\frac{\mathrm{d}m_\mathrm{b}}{\mathrm{d}t} \tag{1}$$

$$\frac{\mathrm{d}(m_\mathrm{u}u_\mathrm{u})}{\mathrm{d}t} = -P\frac{\mathrm{d}V_\mathrm{u}}{\mathrm{d}t} + \frac{\mathrm{d}m_\mathrm{u}}{\mathrm{d}t}h_\mathrm{u} + \frac{\mathrm{d}Q_\mathrm{u}}{\mathrm{d}t} \tag{2}$$

$$\frac{\mathrm{d}(m_\mathrm{b}u_\mathrm{b})}{\mathrm{d}t} = -P\frac{\mathrm{d}V_\mathrm{b}}{\mathrm{d}t} + \frac{\mathrm{d}m_\mathrm{b}}{\mathrm{d}t}h_\mathrm{b} + \frac{\mathrm{d}Q_\mathrm{b}}{\mathrm{d}t} \tag{3}$$

As same pressure is considered in both the burned zone and the unburned zone, Equation (4) can be established:

$$P = \frac{m_\mathrm{b}R_\mathrm{b}T_\mathrm{b}}{V_\mathrm{b}} = \frac{m_\mathrm{u}R_\mathrm{u}T_\mathrm{u}}{V_\mathrm{u}} \tag{4}$$

From the above four equations, the following equations can be derived:

$$\frac{\mathrm{d}T_\mathrm{u}}{\mathrm{d}t} = \frac{1}{m_\mathrm{u}c_\mathrm{pu}}\left(V_\mathrm{u}\frac{\mathrm{d}P}{\mathrm{d}t} + \frac{\mathrm{d}Q_\mathrm{u}}{\mathrm{d}t}\right) \tag{5}$$

$$\frac{\mathrm{d}T_\mathrm{b}}{\mathrm{d}t} = \frac{1}{m_\mathrm{b}R_\mathrm{b}}\left[P\frac{\mathrm{d}V}{\mathrm{d}t} - (R_\mathrm{b}T_\mathrm{b} - R_\mathrm{u}T_\mathrm{u})\frac{\mathrm{d}m_\mathrm{b}}{\mathrm{d}t} - \frac{R_\mathrm{u}}{c_\mathrm{pu}}\left(V_\mathrm{u}\frac{\mathrm{d}P}{\mathrm{d}t} + \frac{\mathrm{d}Q_\mathrm{u}}{\mathrm{d}t}\right) + V\frac{\mathrm{d}P}{\mathrm{d}t}\right] \tag{6}$$

$$\frac{\mathrm{d}p}{\mathrm{d}t} = \frac{-\left[(u_\mathrm{b} - u_\mathrm{u}) - c_\mathrm{vb}\left(T_\mathrm{b} - T_\mathrm{u}\frac{R_\mathrm{u}}{R_\mathrm{b}}\right)\right]\frac{\mathrm{d}m_\mathrm{b}}{\mathrm{d}t} - \left(\frac{c_\mathrm{vu}}{c_\mathrm{pu}} - \frac{c_\mathrm{vb}}{c_\mathrm{pu}}\frac{R_\mathrm{u}}{R_\mathrm{b}}\right)\frac{\mathrm{d}Q_\mathrm{u}}{\mathrm{d}t} + \left(\frac{\mathrm{d}Q_\mathrm{u}}{\mathrm{d}t} + \frac{\mathrm{d}Q_\mathrm{b}}{\mathrm{d}t}\right)}{V_\mathrm{u}\left(\frac{c_\mathrm{vu}}{c_\mathrm{pu}} - \frac{c_\mathrm{vb}}{c_\mathrm{pu}}\frac{R_\mathrm{u}}{R_\mathrm{b}}\right) + V\frac{c_\mathrm{vb}}{R_\mathrm{b}}} \tag{7}$$

where the heat transfer rate $\mathrm{d}Q_\mathrm{u}/\mathrm{d}t$ and $\mathrm{d}Q_\mathrm{b}/\mathrm{d}t$ are estimated from Annand's formulas [27]. With respect to model calculation, $\mathrm{d}P/\mathrm{d}t$ is obtained from the pressure data in the experiments and $\mathrm{d}V/\mathrm{d}t$ takes the value zero for the constant volume bomb. The internal energy and various gas constants of mixtures are calculated using the formula given by the literature according to the fraction of each species [28]. The initial burned gas temperature uses the adiabatic flame temperature, and using a fourth-order Runge-Kutta scheme, the unknown variables in these thermodynamic equations m_b, T_b, T_u, and $\mathrm{d}m_\mathrm{b}/\mathrm{d}t$ can be obtained. During the combustion process, gas compositions and properties are calculated through chemical equilibrium with 11 species and seven equations [29].

3. Results and Discussion

3.1. Numerical Study on Electric Field Distributions

In the experiment, the spatial electric field distributions at various input voltages are simulated using ANSYS 13.0. For simplicity, Figure 3 only shows the electric field distributions in the vertical cross section along the bomb centerline at the input voltage of −12 kV.

It can be seen in Figure 3 that the electric fields produced by the high-voltage electrodes are typically non-uniform but their distributions are all symmetrical. The electric field strengths in the

horizontal direction are more intense than that in the vertical direction. Meanwhile, the direction of the electric field line mostly points horizontally to the high-voltage electrodes from the vertical bomb centerline and the bomb circumference.

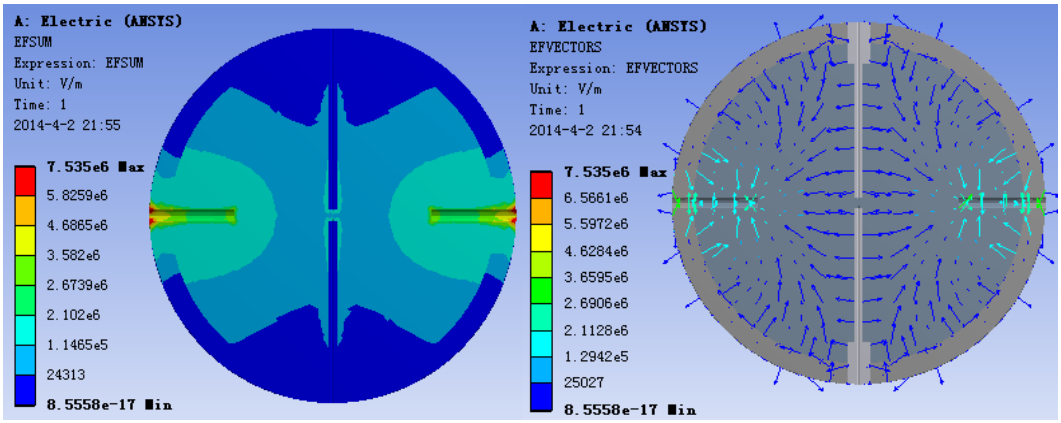

Figure 3. Electric field distributions at input voltage of −12 kV.

Figure 4 shows the value of electric field strength along the bomb horizontal centerline between the high-voltage electrodes at the input voltage of −12 kV. The electric field strength of each position can be obtained from Figure 4, and the mean value of the electric field strength is defined as the ratio of the sum of the electric field strength of each position to the number of the electric field strength position. It can be seen that the value of the electric field strength almost monotonous increases from 0.14×10^5 V/m (located in the ignition electrodes) to 2.95×10^6 V/m (located in the high-voltage electrodes). While the electric fields in the region within 27 mm away from the center are relatively uniform, its mean value being about 1.45×10^5 V/m, However, in the region close to the needle tip, the electric field intensity increases significantly, reaching about 2.95×10^6 V/m from 2.7×10^5 V/m in an interval distance of about 8 mm. The changing trends of the electric field strength at the input voltage of −5 kV and −10 kV are in consistent with that at −12 kV due to the electric field strength proportional to the applied voltages.

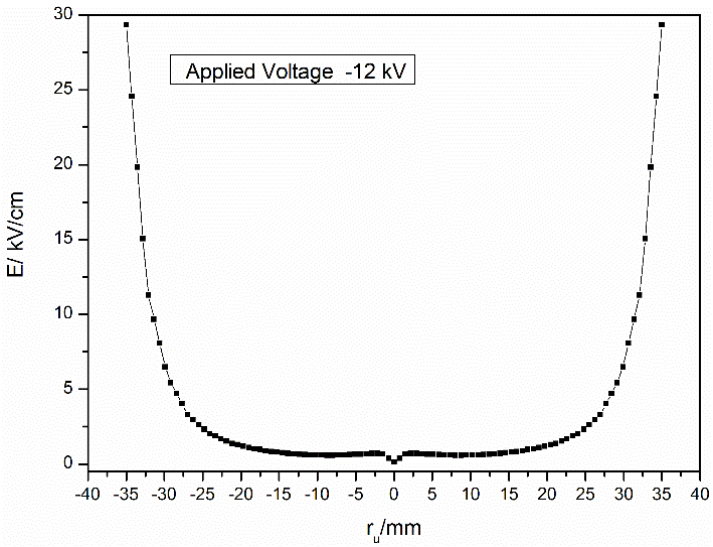

Figure 4. The electric field strength *versus* the horizontal distance for the case at −12 kV.

3.2. Influence of the Electric Field on the Flame Shape Modification

Figure 5 shows images of flame propagation processes at λ = 1.2, 1.4 and 1.6 under the various applied electric fields. The input voltages and the elapsed times after ignition are correspondingly tabulated beside the relevant flame images. At an input voltage of 0 kV, *i.e.*, in the absence of electric fields, the flame front at any excess air ratio is almost spherical shape and propagates evenly in both horizontal and vertical directions. It also can be seen that the flame propagates relatively slower when the mixture becomes leaner. When the input voltage is −5 kV, the flame front in the horizontal direction is slightly stretched, whereas the flame front almost remains spherical in shape, and the flame surface almost keeps smooth in the process of the flame development. While, when the applied voltage increases to −10 kV, or −12 kV, the horizontal flame front is lengthened markedly and propagates evenly in both the rightward and leftward direction, whereas the vertical flame propagation changes little. In the case of the three excess air ratios, there is an apparent discrepancy between the changes in the flame shape. For λ = 1.2, the flame front shape changes little, and almost retains its previous spherical flame front, while for λ = 1.4 and 1.6, due to the flame front in the horizontal direction is prolonged remarkably, the flame front takes on a prolate sphere shape.

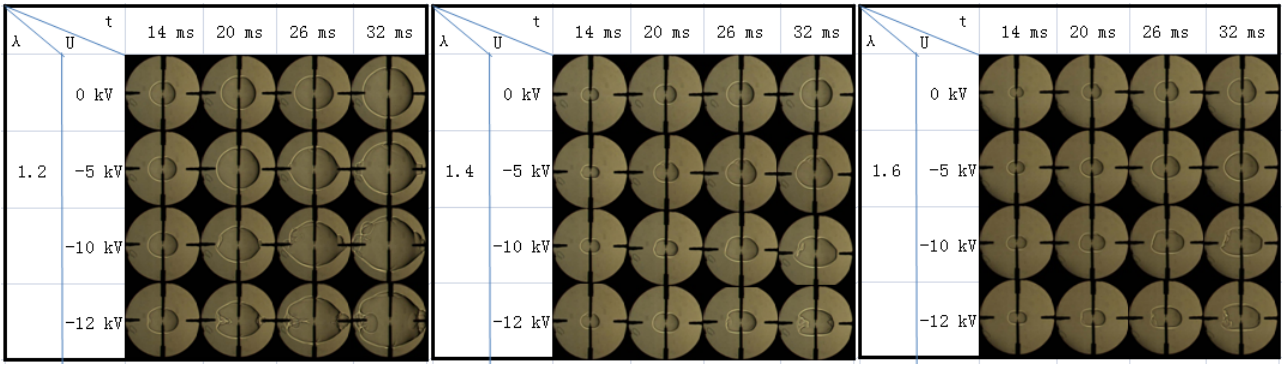

Figure 5. Images of flame propagation process at excess air ratio of λ = 1.2, 1.4, and 1.6.

The lengthening of the flame front in the horizontal direction under the electric field is primarily ascribed to the ionic wind effect, *i.e.*, a bulk flow movement due to electric-field-induced directional collisions of ions and neutral molecules in flame front [11,12]. It is accepted that the positive ions such as H_3O^+, $C_2H_4^+$ and CHO^+ formed in the methane flame contribute more to the ion molecule collision because of their abundance and greater mass compared with electrons [14]. The ionic wind effect, which increases with electric field intensity and particle number density, generates the momentum transfer of positive ions and the acceleration of neutral molecules with which the ions collide. As a consequence, the ion-neutral collisions within the flame front, the flame propagates more rapidly in the field direction compared to that in the other orientations. As shown in Figure 3, the applied electric fields are almost horizontally oriented toward the two high-voltage electrodes from the vertical bomb centerline, and the magnitude of the electric field in the horizontal direction is more intense than that in the vertical direction. This indicates that the applied electric field can noticeably accelerate the horizontal flame propagation and stretch the flame front, but has little influence on the vertical flame propagation. Moreover, the electric field enhances the flame propagation from a low input voltage, and

the effect gradually increases as the input voltage increases. This results in that the flame shape deforms more significant at high input voltage.

It can be also seen that under the applied electric field, the flame shape modifies more pronounced for the leaner mixture. This can be explained by the fact that the ionic wind effect on the flame development can be relevant to the flame propagation status itself. For leaner mixture, flame propagation would take more time within a certain distance due to its slow flame propagation. This would lengthen the period of the applied electric field influence on the combustion process. According to the theory of ionic wind effect [22], the amount of accelerated neutral molecules which have collided with the positive ions and gained momentum from them will be increased when the available time is lengthened, and this can markedly enhance the effect of the electric field on flame propagation. In the case of the relatively slow propagation speed without electric field, the increase rate of the flame propagation can be great under the electric field. As a consequence, the stretch of the flame front is relatively larger and the flame shape modification is more significant for the leaner mixture.

3.3. Influence of the Electric Field on Flame Propagation Velocity

As shown in Figure 5, the flame front propagation can change greatly under the applied electric field. For the three excess air ratios studied here, the flame front propagation in the horizontal direction is remarkably accelerated, while the vertical flame propagation is weakly affected. Therefore, the horizontal flame speed is investigated to elucidate the influence of the applied electric fields on flame propagation. The stretched flame propagation velocity S_n, reflecting the flame moving speed relative to the motionless combustion wall, is derived from the flame propagation radius *versus* time, $S_n = \frac{dr_u}{dt}$. where, r_u is the horizontal flame radius and t is the elapsed time after spark ignition. In this paper, for the sake of more accurately calculating S_n, r_u is defined as the mean value of various flame radius from the ignition center to the flame front at the set polar angles of 0°, ±15°, ±165° and 180°, respectively, as shown in Figure 6. Previous studies showed the ignition energy gave an important influence on the flame at the initial stage of the combustion. While as the flame radius is larger than 5 mm, the influence would disappear [30]. In addition, in order to avoid the wall and pressure influence (the pressure rise rate is less than 1.0%) in the combustion chamber, the analysis of the flame radius is limited to 25 mm [30]. The data in this study use those of the flame radius from 5 to 25 mm.

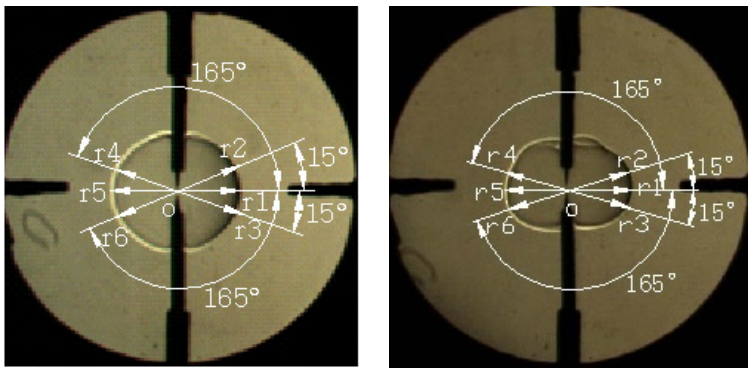

(**a**) (**b**)

Figure 6. Data obtained from a flame image. (**a**) Spherical flame, (**b**) Stretched flame.

Figure 7 gives the variations of flame radius *versus* the time under the electric field. The excess air ratios are 1.2, 1.4 and 1.6, and the input voltages are 0 kV, −5 kV, −10 kV and −12 kV, respectively. For an input voltage of 0 kV, the flame radius increases almost linearly with time and the flame propagates slower as the excess air ratio is increased. Under the applied electric field, the flame radius at a given time is larger than that without electric field, indicating that the input electric field can enhance flame propagation. Additionally, the higher the input voltage, the faster the flame propagates. For the three excess air ratios, the increase in the flame propagation at λ = 1.6 is the largest, and that for λ = 1.4 and 1.2 the less large in return. For example, at the input voltage of −12 kV, when r_u increases to 25 mm, the corresponding time are 12.74, 17.53 and 23.96 ms for λ = 1.2, 1.4 and 1.6,which are advanced by 23.7%, 31.1% and 37.0%, respectively, compared to that when no electric field is applied. These results further reveal that the electric field can significantly stretch the flame front as the input voltage increases, and this phenomenon is the more obvious for leaner mixture.

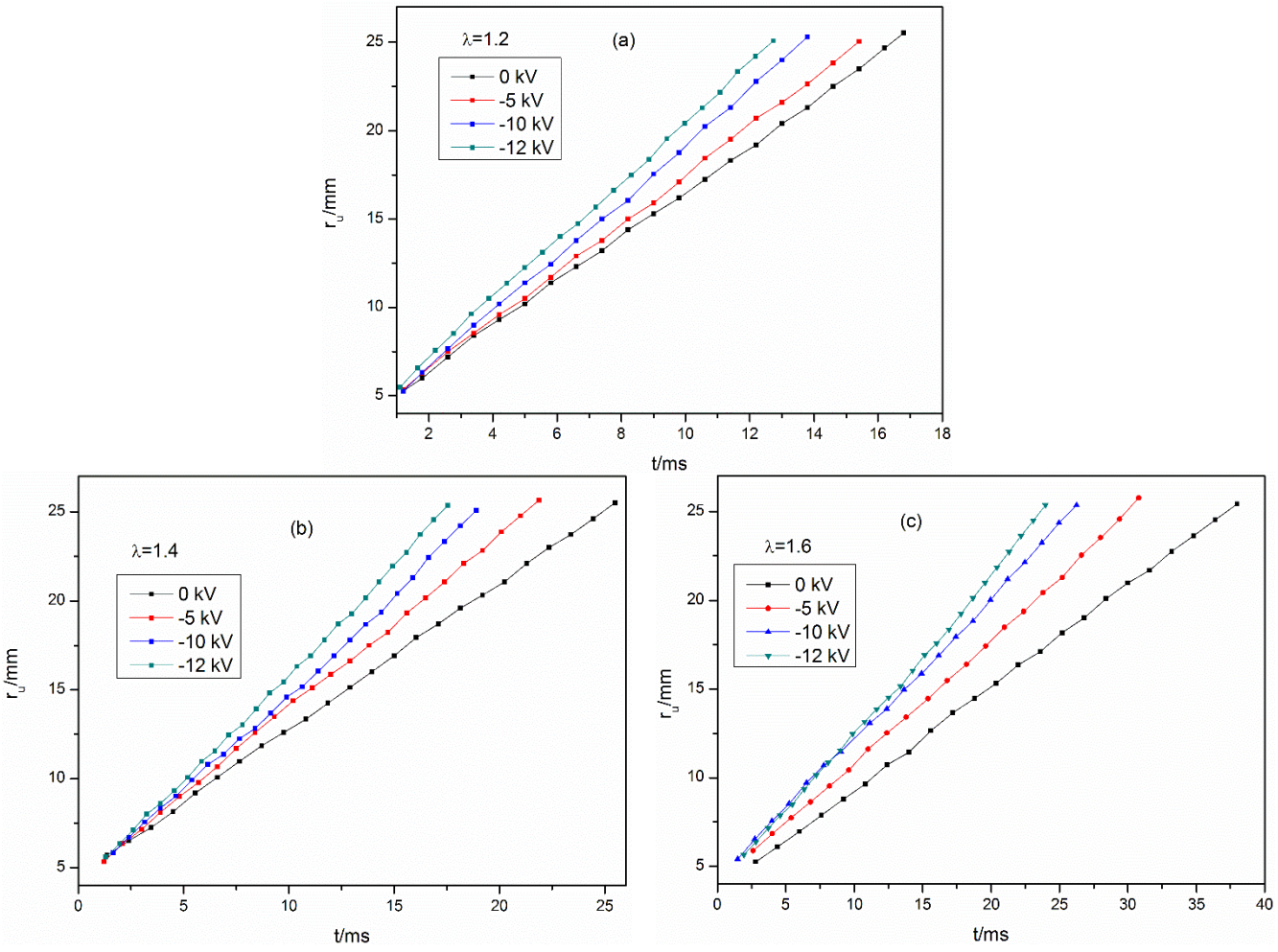

Figure 7. Flame radius *versus* combustion time under various conditions. (**a**) λ = 1.2, (**b**) 1.4, and (**c**) 1.6 with the voltages of 0, −5, −10, −12 kV.

Figure 8 gives the relationship between the stretched flame propagation velocity S_n and the flame radius r_u. In the absence of applied voltage for each excess air ratio, the stretched flame propagation velocity increases slightly with the increase of flame radius, and our experiment results are concordant with that cited in the previous literature [30,31]. Under the influence of the electric field, S_n for any

excess air ratio increases rapidly compared with the case without electric field, and the effects are increased with the input voltage increase. The peak values of S_n are 1.86, 1.34 and 1.06 m/s, occurring at voltage of −12 kV, for λ = 1.2, 1.4 and 1.6, and they are increased by 34%, 56%, 67% compared to the case of no electric field, respectively. Additionally, the influence of the electric field on S_n increases with the flame propagation. The enhancement of S_n can be ascribed to the field-induced flame stretch due to the ionic wind effect, whose increase tendency is concordant with the increase of the corresponding flame radius under the same conditions.

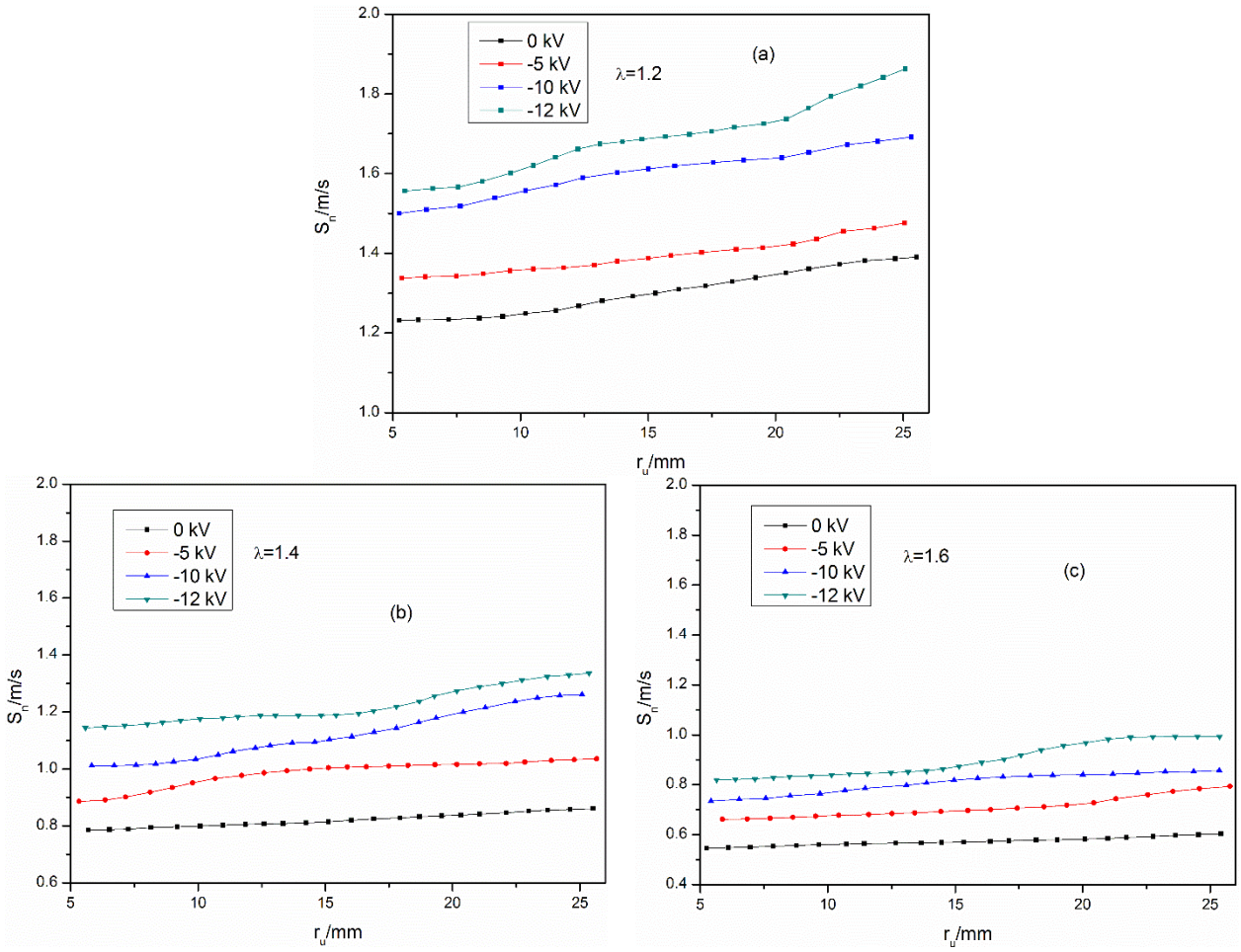

Figure 8. Stretched flame propagation velocity *versus* flame radius under various conditions. (**a**) λ = 1.2, (**b**) 1.4, (**c**) 1.6 with the voltages of 0, −5, −10, −12 kV.

From above the flame shape changes and the increase of the stretched flame propagation velocity, it can be seen that the flame development can be influenced by these so-called stretched effects induced by the electric field. The stretch in flame comprises hydrodynamic stretch and flame stretch. Their detailed definition can be found in Reference [32]; here we directly adopt the relevant concepts. The hydrodynamic stretch, through the combined effects of the tangential and normal velocity gradient at the flame, displaces the flame surface, distorts the flame geometry, and modifies the volumetric burning rate. The positive hydrodynamic stretch pointes in the upstream direction of the flame (toward the unburned zone), while the negative hydrodynamic stretch pointes in the downstream direction of the flame (toward the burnt zone). The flame stretch can directly affect the normal mass flux entering

the reaction zone by the tangential velocity variation in the transport zone. Moreover, through interaction with heat and mass diffusion, the flame stretch can modify the temperature and concentration profiles in the transport zone and consequently the burning intensity. During the flame propagation, the flame stretch and hydrodynamic stretch are strongly coupled in flame, and can affect the flames responses and structure. The present experimental data show that the flame front in the electric field direction is stretched and form the pocket regime convex towards unburned gas. The phenomena indicate that the applied electric field can augment the positive hydrodynamic stretch in flame. In addition, the increase rate of the flame radius propagation at λ = 1.6 is the largest, that for λ = 1.4 the less large and that for λ = 1.2 the smallest. Meanwhile, the increase rate of the corresponding stretched flame propagation velocity also show same change trend. This shows the electric field-induced stretch is enhanced with the increase of input voltage, and the result is relatively greater for leaner mixture.

For the sake of comparison of the effects of the applied electric field on the laminar flame speed as a whole, Table 1 gives the average flame propagation velocity S_m at λ = 1.2, 1.4, 1.6 and their increase rate ΔS_m under different input voltages. S_m is calculated by $S_m = (r_2 - r_1)/(t_2 - t_1)$, in which, r_1 = 5 mm, r_2 = 25 mm, t_1 and t_2 is the time that the flame radius increases to r_1 and r_2, respectively. ΔS_m is defined as follow: $\Delta S_m = \frac{S_m - S_{m0}}{S_{m0}} * 100\%$, where S_m and S_{m0} are the average flame propagation velocity for the case at a certain input voltage and 0 kV, respectively. Without the applied voltage, S_m gives its maximum value at λ = 1.2, and the value at λ = 1.4 and 1.6 decreases in turn progressively. When the input voltage is applied to the mixtures at any excess air rate, S_m increases steadily with the increase of the input voltage. Moreover, ΔS_m for λ = 1.6 is the biggest, while its value becomes less big for λ = 1.4 and 1.2 successively. For example, at the applied voltage of −12 kV, S_m for λ = 1.2, 1.4, and 1.6 are 1.69, 1.22, and 0.9 m/s, and their corresponding ΔS_m are 30.0%, 48.8% and 57.9%, respectively. The result indicates the electric field can enhance the flame laminar speed, and the improvement effect is more pronounced when the mixture becomes leaner.

Table 1. Average flame propagation velocity (m/s) and its increase rate for various excess air ratios.

U (kV)	λ = 1.2		λ = 1.4		λ = 1.6	
	S_m (m/s)	ΔS_m (%)	S_m (m/s)	ΔS_m (%)	S_m (m/s)	ΔS_m (%)
0	1.30	0	0.82	0	0.57	0
−5	1.39	6.9	0.98	19.5	0.71	24.6
−10	1.59	22.3	1.12	36.6	0.80	40.4
−12	1.69	30.0	1.22	48.8	0.90	57.9

3.4. Influence of the Electric Field on Peak Combustion Pressure

Figure 9 shows the combustion pressure traces under the application of the electric field. The excess air ratios are 1.2, 1.4 and 1.6 and the input voltages are 0 kV, −5 kV, −10 kV, and −12 kV, respectively. It can be seen that in the case of no electric field, the combustion process grows slower with the excess air ratio increasing. In addition, the corresponding value of peak pressure decreases and the timing of the peak pressure is delayed. When the electric field is applied to the mixture at any excess air ratio, the combustion pressure increases rapidly in the early stage and the corresponding value is higher than

that without electric fields. Moreover, the peak combustion pressure increases and the timing of the peak pressure is remarkably advanced compared with that in the absence of the electric field. The higher the input voltage, the greater effect of the applied electric field on combustion pressure is. Table 2 shows the maximum combustion pressure P_{max}, the timing of maximum pressure appearance t_p, and their increase rates ΔP_{max} and Δt_p which compared to the corresponding case of no electric field. It can be seen that the largest increase of P_{max} and the most significant advancement of t_p are presented at $\lambda = 1.6$, that for $\lambda = 1.4$ the less pronounced and that for $\lambda = 1.2$ the smallest. For example, at the input voltage of −12 kV, P_{max} increases by 5.1%, 5.9% and 12.3%, and t_p is advanced by 20.8%, 25.2% and 31.8%, for $\lambda = 1.2$, 1.4 and 1.6, respectively, compared to the corresponding case of no electric fields.

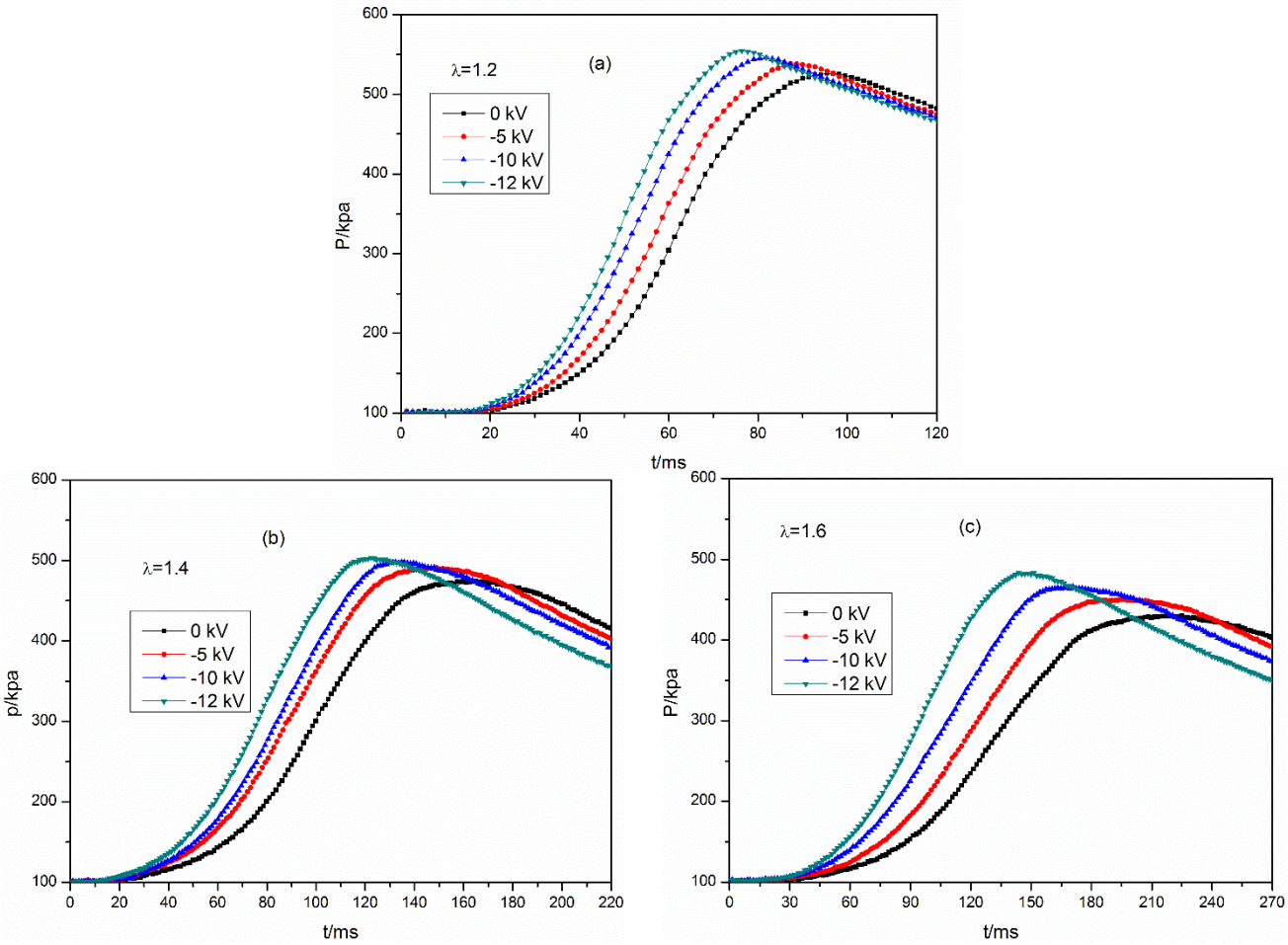

Figure 9. The combustion pressure records under various conditions. (**a**) λ = 1.2, (**b**) 1.4, (**c**) 1.6 with the voltages of 0, −5, −10, −12 kV.

Table 2. Combustion characteristics and the increase rates for various excess air ratios.

U (kV)	λ = 1.2				λ = 1.4				λ = 1.6			
	P_{max} (kPa)	ΔP_{max} (%)	t_P (ms)	Δt_P (%)	P_{max} (kPa)	ΔP_{max} (%)	t_P (ms)	Δt_P (%)	P_{max} (kPa)	ΔP_{max} (%)	t_P (ms)	Δt_P (%)
0	527.7	0	95.8	0	475.2	0	163.8	0	430.4	0	217.2	0
−5	538.8	2.1	89.5	−6.6	491.7	3.5	144.5	−11.8	450.5	4.7	191.8	−11.7
−10	546.9	3.7	81.6	−14.7	498.4	4.9	133.9	−18.2	465.9	8.3	167.5	−22.9
−12	554.7	5.1	75.8	−20.8	503.4	5.9	122.5	−25.2	483.5	12.3	148.1	−31.8

The previous sections of this paper concerning the flame propagation have shown that the applied electric fields can accelerate the flame propagation velocity, and the effects increase with the increase of the input voltage. Thus, the whole combustion process is accelerated compared with the case of no electric field. As a consequence, the combustion pressure in initial stage period grows up fast and high, and t_p at any excess air ratio is advanced obvious. The larger the increase of flame propagation speed, the greater t_p is advanced. The increase of peak combustion pressure under the influence of applied electric field is most likely related to the heat release of combustion and the heat loss to the bomb [24]. As stated before, the applied electric field can augment the positive hydrodynamic stretch in flame (toward the unburned zone), and this result will increase the local volumetric burning rate. Additionally, in the region near the needle tip with intense electric field, the ionic wind effects induce the flame front to appear wrinkles and distortions, and this further enlarge the flame front area and improve the burning rate of combustible mixture. On the other hand, the field-induced flame stretch can strongly influence the flame response and structure for mixtures with unequal diffusivities [32]. For a stretched flame, the reaction zone in the stretched surface loses thermal energy to the external unburned gas while it gains chemical energy from them due to an increase of deficient reaction concentration. Thus the stretched flame behavior, especially its temperature, depends on the relative rates of heat and mass diffusion. According to the combustion theory, Lewis number (Le) is defined as the ratio of heat diffusivity of the mixture to the mass diffusivity of the deficient reactant. If the heat loss and mass gain are equal such that Le = 1, then the total energy is conserved and the flame temperature is the adiabatic temperature. However, if mass gain exceeds heat loss (Le < 1), then there will be more intensified burning on the stretched surface such that the flame temperature is higher than the adiabatic temperature. Conversely, if Le > 1, the flame temperature is lower than the adiabatic flame temperature. In the case of lean methane-air mixture, Le < 1, *i.e.*, the mass diffusion exceeds the thermal diffusion. Based on the influence of the non-unity Lewis number in the burning intensity of stretched flames, the field-induced flame stretch will cause the burning more strong and the flame temperature increase. Previous studies [32,33] conducted on methane–air flames also demonstrated that the positive flame stretch can lead to the flame temperature increase at Le < 1. This argument still holds even if we just consider the relative mass diffusivities of the fuel and oxidizer. Based on molecular weight considerations, the diffusivities of methane and oxygen relative to nitrogen decrease in turn. Thus positive flame stretch will increase the methane concentration of a lean methane-air mixture at the flame. The reaction zone is consequently rendered more stoichiometric, leading to the enhanced burning intensity. In addition, the increase of flame speed under the electric field markedly enhances the whole combustion process, and shortens the overall combustion duration. Therefore, the heat loss from the flame to the bomb wall could decrease. The combined influence of the above factors gives P_{max} increase relative largely for lean methane–air mixtures. The effect of the electric field on combustion pressure at leaner mixture is more pronounced because the electric field-induced stretch in flame is relatively greater in this case.

3.5. Influence of the Electric Field on the Heat Release Rate

In order to further figure out the effect of the applied electric field on the combustion process, Figure 10 gives the normalized mass burning rate at λ = 1.2, 1.4 and 1.6 under various input voltages.

In this paper, the normalized mass burning rate is defined as $(1/m)(dm_b/dt)$, which is calculated based upon foregoing two-zone mode and reflects the burning velocity of the mixture during the combustion process. In the absence of the electric field, the normalized mass burning rate curve has a single peak at any excess air ratio. This illustrates the combustion process flame in the constant volume bomb is mainly based on the premixed mixture burning. For the three excess air ratios, the fast rate and high value of the normalized mass burning rate are presented at λ = 1.2, and the slow rate and low value of the normalized mass burning rate are demonstrated at λ = 1.4 and 1.6 in turn. Under the application of the electric field, the normalized mass burning rate grows up fast, and the whole combustion duration is shortened. Thus, the peak value of the normalized mass burning rate increases, and its appearance time is advanced. Moreover, the enhancement of the normalized mass burning rate for λ = 1.6 is most significant, followed by that at λ = 1.4 and 1.2 in turn. For example, at the applied voltage of −12 kV, the peak value of the normalized mass burning rate increases by almost 9.3%, 16.6% and 28.9%, and its appearance times are advanced by almost 18.5%, 20.2% and 25.4%, for λ = 1.2, 1.4 and 1.6, respectively, when compared to the corresponding case of no electric fields. These results further verify that the electric field can significantly enhance the combustion process of the lean methane–air mixture, and this impact is more pronounced when the excess air ratio is increased. These effects are consistent to the behaviors of pressure records for the three excess air ratios under the electric field.

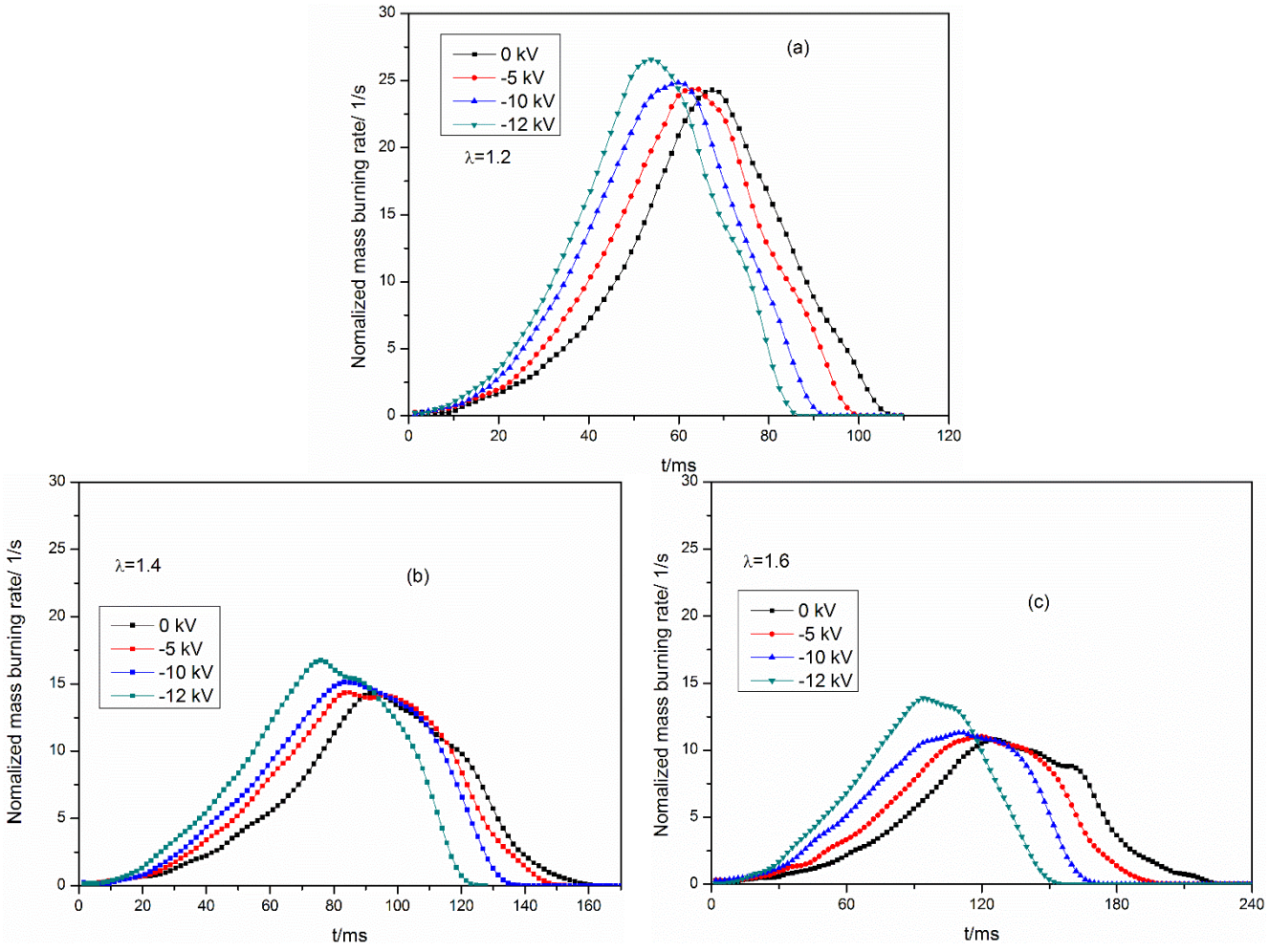

Figure 10. Nomalized mass burning rate under various conditions. (**a**) λ = 1.2, (**b**) 1.4, (**c**) 1.6 with the voltages of 0, −5, −10, −12 kV.

Figure 11 gives the accumulated mass fraction burned at λ = 1.2, 1.4, and 1.6 under various input voltages. When the electric field is applied to the mixture at any excess air ratio, the accumulated mass fraction burned grows up fast with the increase of the applied voltage due to the increase of flame propagation speed. According to the combustion theory, the flame development duration (t_a) is the time interval from the spark ignition to the timing that 10% of mass fraction burned is reached; the rapid combustion duration (t_b) is the time interval from 10% mass fraction burned to the timing of 90% mass fraction burned. Table 3 shows t_a, t_b, and their increase rates Δt_a and Δt_b which compared to the corresponding case without electric field. As can be seen, both t_a and t_b are all reduced with the increase of the applied voltage, and the effect for leaner mixture is more significant. For example, at the input voltage of −12 kV, t_a are decreased by almost 22.3%, 26.2% and 31.5%, and t_b are decreased by 12.6%, 16.0% and 20.8%, for λ = 1.2, 1.4 and 1.6, respectively, compared to the corresponding case of without electric field. This reveals the fact the electric field can enhance the burning speed of the lean methane-air mixture, especially it gives larger influence on decreasing the flame development duration.

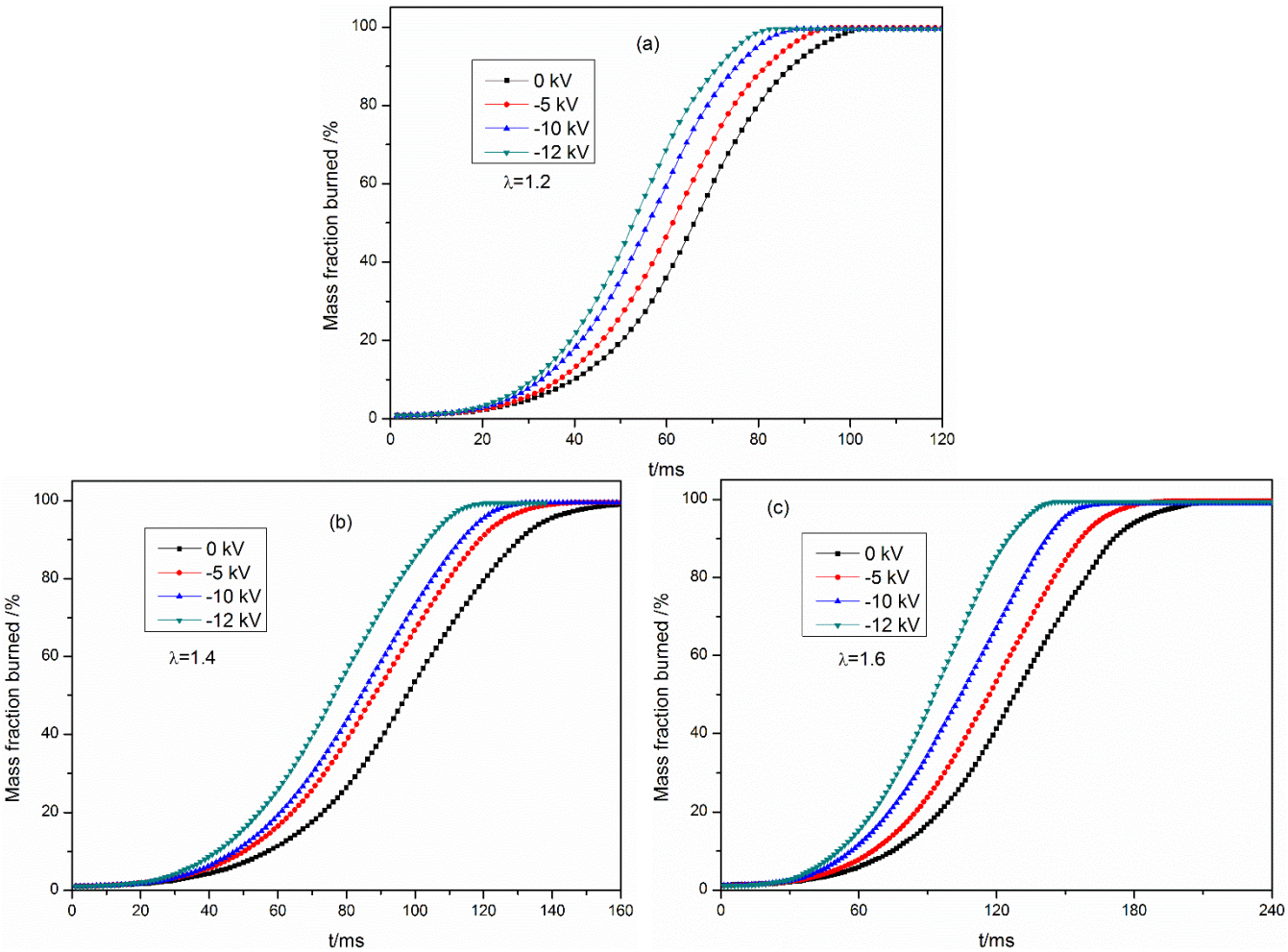

Figure 11. Mass fraction burned as a function of time under various conditions. (**a**) λ = 1.2, (**b**) 1.4, (**c**) 1.6 with the voltages of 0, −5, −10, −12 kV.

Table 3. Flame development duration and rapid combustion duration and their increase rates for λ = 1.2, 1.4 and 1.6.

U (kV)	Flame Development Duration						Rapid Combustion Duration					
	λ = 1.2		λ = 1.4		λ = 1.6		λ = 1.2		λ = 1.4		λ = 1.6	
	t_a (ms)	Δt_a (%)	t_a (ms)	Δt_a (%)	t_a (ms)	Δt_a (%)	t_b (ms)	Δt_b (%)	t_b (ms)	Δt_b (%)	t_b (ms)	Δt_b (%)
0	39.9	0	57.3	0	74.7	0	47.5	0	73.3	0	96.6	0
−5	36.7	−8.0	51.8	−9.6	66.2	−11.4	45.2	−4.8	69.5	−5.2	90.7	−6.1
−10	32.8	−17.8	46.1	−20.0	56.2	−24.8	43.2	−9.1	66.0	−10.0	85.2	−11.8
−12	31.0	−22.3	42.3	−26.2	51.2	−31.5	41.5	−12.6	61.6	−16.0	76.5	−20.8

4. Conclusions

(1) The electric field distributions created by the high-voltage electrodes are symmetrical and their directions point to the high voltage electrodes from the bomb circumference and the vertical bomb centerline. The electric field strengths in the horizontal direction are more intense than that in the vertical direction. The horizontal electric fields in the region within 27 mm away from the center are relatively uniform, while its value vicinal the needle tip is relatively large.

(2) When the electric field is applied, the flame front is stretched remarkably in the direction of the electric field, the stretched flame propagation velocity and the average flame propagation velocity are accelerated significantly as the input voltage increases. For various excess air ratios, the increase of the flame speed for λ = 1.6 is the largest, followed by that for λ = 1.4 and 1.2. This indicates the electric field can augment the stretch in flame, and the behavior is more pronounced when the mixture becomes leaner.

(3) When the electric field is applied, the combustion peak pressure is increased and its appearance time is advanced compared with the case of no electric fields. For the heat release rate, the normalized mass burning rate and the accumulated mass fraction burned are all improved substantially, the flame development duration and the rapid burning duration are remarkably reduced with the increase of the input voltage. Moreover, the electric field shows larger influence on the combustion characteristics for the leaner mixtures.

Acknowledgments

The authors gratefully acknowledge the National Natural Science Foundation of China (Grants No. 51476126 and 51176150), State Key Laboratory of Automotive Safety and Energy, Tsinghua University (Grant No. KF14122).

Author Contributions

Jianfeng Fang carried out all the experiments and wrote the manuscript. Xiaomin Wu designed all the experiments and revised the manuscript. Hao Duan performed the semi-continuous experiment. Chao Li performed the batch experiment. Zhongquan Gao designed the experiment and edited the manuscript.

Nomenclature

c_p	constant pressure specific heat of the mixture, kJ/(kg·K)
h	enthalpy, J
c_v	constant volume specific heat of the mixture, kJ/(kg·K)
m	mass, kg
Q	heat loss, J
T	gas temperature, K
V	volume, m^3
u	Internal energy, J
t	elapsed time from ignition, ms
R	gas constant, J/(g·K)
P	pressure, Pa
λ	excess air ratio
S_n	stretched flame propagation velocity, m/s
r	flame radius, mm
S_m	average flame propagation velocity, m/s
t_a	flame development duration, ms
t_b	rapid combustion duration, ms
t_p	timing of maximum pressure, ms

Subscripts

u	Unburned gas
b	Burned gas

Conflicts of Interest

The authors declare no conflict of interest.

References

1. Wisman, D.L.; Marcum, S.D.; Ganguly, B.N. Electrical control of the thermo diffusive instability in premixed propane-air flames. *Combust. Flame* **2007**, *151*, 639–648.
2. Kim, M.K.; Chung, H.S.; Kim, H.H. Effect of AC electric fields on the stabilization of premixed bunsen flames. *Proc. Combust. Inst*. **2011**, *33*, 1137–1144.
3. Altendorfner, F.; Kuhl, J.; Zigan, L. Study of the influence of electric fields on flames using planar LIF and PIV techniques. *Proc. Combust. Inst.* **2011**, *33*, 3195–3201.
4. Calcote, H.F.; Pease, R.N. Electrical properties of flames-Burner flames in longitudinal electric fields. *Ind. Eng. Chem*. **1951**, *43*, 2726–2731.
5. Lee, S.M.; Park, C.S.; Cha, M.S.; Chung, S.H. Effect of electric fields on the liftoff of non-premixed turbulent jet flames. *IEEE Trans. Plasma Sci*. **2005**, *33*, 1703–1709.
6. Kim, M.K.; Ryu, S.K.; Won, S.H.; Chung, S.H. Electric fields effect on lift off and blow off of nonpremixed laminar jet flames in a coflow. *Combust. Flame* **2010**, *157*, 17–24.

7. Yamashita, K.; Karnani, S.; Dunn-Rankin, D. Numerical prediction of ion current from a small methane jet flame. *Combust. Flame* **2009**, *156*, 1227–1233.
8. Volkov, E.N.; Sepman, A.V.; Kornilov, V.N.; Konnov, A.A.; Shoshin, Y.S.; de Coey, L.P.H. Towards the mechanism of DC electric field effect on flat premixed flame. In Proceedings of the European Combustion Meeting, Vienna, Austria, 14–17 April 2009.
9. Won, S.H.; Cha, M.S.; Park, C.S.; Chung, S.H. Effect of electric fields on reattachment and propagation speed of tribrachial flames in laminar coflow jets. *Proc. Combust. Inst*. **2007**, *31*, 963–970.
10. Vandenboom, J.; Konnov, A.; Verhasselt, A.; Kornilov, V.; Degoey, L.; Nijmeijer, H. The effect of a DC electric field on the laminar burning velocity of premixed methane/air flames. *Proc. Combust. Inst.* **2009**, *32*, 1237–1244.
11. Sanchez-Sanz, M.; Murphy, D.C.; Fernandez-Pello, C. Effect of an external electric fields on the propagation velocity of premixed flames. *Proc. Combust. Inst.* **2015**, *35*, 3463–3470.
12. Hu, J.; Rivin, B.; Sher, E. The effect of an electric field on the shape of co-flowing and candle-type methane–air flames. *Exp. Therm. Fluid Sci.* **2000**, *21*, 124–133.
13. Memdouh, B.; Pascal, D.; Pierre, V. Direct numerical simulation of the effect of an electric field on flame stability. *Combust. Flame* **2010**, *157*, 2286–2297.
14. Moriya, S.; Yoshida, K.; Shoji, H.; Iijima, A. The effect of uniform and non-uniform electric fields on flame propagation. *J. Therm. Sci. Technol*. **2008**, *3*, 254–265.
15. Vega, E.V.; Lee, K.Y. An experimental study on laminar $CH_4/O_2/N_2$ premixed flames under an electric field. *J. Mech. Sci. Technol.* **2008**, *22*, 312–319.
16. Marcum, S.D.; Ganguly, B.N. Electric-field-induced flame speed modification. *Combust. Flame* **2005**, *143*, 27–36.
17. Ryu, S.K.; Kim, Y.K.; Kim, M.K.; Won, S.H.; Chung, S.H. Observation of multi-scale oscillation of laminar lifted flames with low-frequency AC electric fields. *Combust. Flame* **2010**, *157*, 25–32.
18. Xie, L.; Kishi, T.; Kono, M. The influence of electric fields on soot formation and flame structure of diffusion flames. *J. Therm. Sci*. **1993**, *2*, 288–293.
19. Cha, M.S.; Lee, S.M.; Kim, K.T.; Chung, S.H. Soot suppression by nonthermal plasma in coflow jet diffusion flames using a dielectric barrier discharge. *Combust. Flame* **2005**, *141*, 438–447.
20. Won, S.H.; Ryu, S.K.; Kim, M.K.; Cha, M.S.; Chung, S.H. Effect of electric fields on the propagation speed of tribrachial flames in coflow jets. *Combust. Flame* **2008**, *152*, 496–506.
21. Zake, M.; Barmina, I.; Turlajs, D. Electric field control of polluting emissions from a propane flame. *Global Nest Int. J*. **2001**, *3*, 95–108.
22. Bradley, D.; Nasser, S.H. Electric coronas and burner flames stability. *Combust. Flame* **1984**, *55*, 53–58.
23. Cha, M.S.; Lee, Y. Premixed combustion under electric field in a constant volume chamber. *IEEE Trans. Plasma Sci.* **2012**, *40*, 3131–3138.
24. Meng, X.W.; Wu, X.M.; Kang, C.; Tang, A.D.; Gao, Z.Q. Effects of direct-current (DC) electric fields on flame propagation and combustion characteristics of premixed $CH_4/O_2/N_2$ flames. *Energy Fuels* **2012**, *26*, 6612–6620.

25. Schmidt, J.; Kostka, S.; Lynch, A.; Ganguly, B. Simultaneous particle image velocimetry and chemiluminescene visualization of millisecond-pulsed current-voltage-induced perturbations of a premixed propane/air flame. *Exp. Fluids* **2011**, *51*, 657–665.
26. Kuhl, J.; Jovicic, G.; Zigan, L.; Leipertz, A. Transient electric field response of laminar premixed flames. *Proc. Combust. Inst.* **2013**, *34*, 3303–3310.
27. Liao, S.Y.; Jiang, D.M.; Gao, J.; Zeng, K. Effects of different frequency component in turbulence on accelerating turbulent premixed combustion. *Proc. Inst. Mech. Eng. D* **2003**, *217*, 1023–1030.
28. Heywood, J.B. *Internal Combustion Engine Fundamentals*; McGraw-Hill Book Company: New York, NY, USA, 1988.
29. Shiga, S.; Ozone, S.; Machaacon, H.T.C.; Karasawa, T. A study of the combustion and emission characteristics of compressed-natural gas direction-injection stratified combustion using a rapid compression machine. *Combust. Flame* **2002**, *129*, 1–10.
30. Hu, E.J.; Huang, Z.H.; He, J.J.; Miao, H.Y. Experimental and numerical study on laminar burning characteristics of premixed methane-hydrogen-air flames. *Int. J. Hydrog. Energy* **2009**, *34*, 4876–4888.
31. Liao, S.Y.; Jiang, D.M.; Cheng, Q. Determination of laminar burning velocities for natural gas. *Fuel* **2004**, *83*, 1247–1250.
32. Law, C.K.; Sung, C.J. Structure, aerodynamics, and geometry of premixed flamelets. *Prog. Energy Combust. Sci*. **2000**, *26*, 459–505.
33. Hassan, M.I.; Aung, K.T.; Fasth, G.M. Measured and predicted properties of laminar premixed methane/air flames at various pressures. *Combust. Flame* **1998**, *115*, 539–550.